

Post-pulse dipole instability in adiabatic TDDFT: fact or artifact?

Davood B. Dar,^{1,2} Dhyey Ray,¹ and Neepta T. Maitra¹

¹*Department of Physics, Rutgers University, Newark 07102, New Jersey USA*

²*Department of Physical and Environmental Sciences, University of Toronto, Canada*

(Dated: May 12, 2026)

Recent real-time TDDFT calculations have reported an unexpected delayed growth of molecular dipole oscillations some time after an extreme-ultraviolet (XUV) pulse is applied. We show that numerical and analytical arguments suggest that this instability is an artifact of an incorrect non-linearity introduced by the computational approach: Propagation with an adiabatic exchange-correlation approximation within the time-dependent Kohn-Sham equations of time-dependent density functional theory (TDDFT) tends to amplify initially small and pure sinusoidal oscillations in a system. On the other hand, when this same adiabatic approximation is used within the recent response-reformulated RR-TDDFT, the instability is absent. The absorbing boundary condition plays a crucial role consistent with our argument. We demonstrate this explicitly on the N_2 molecule subject to an XUV pulse, with a range of adiabatic functionals.

I. INTRODUCTION

Predictive computational modeling of molecular processes far from their equilibrium requires a reliable method to capture both correlated electronic motion as well as coupling to ions. At the shortest timescales the electronic dynamics is of prime importance, and significantly influences the subsequent motion of the heavier nuclei. Even neglecting the nuclear motion, solving the full time-dependent Schrödinger equation (TDSE) for the many-electron wavefunction is impossible beyond a few electrons, and one typically resorts to reduced descriptions and approximations of interaction terms. Time-dependent density functional theory (TDDFT) has emerged as the most practical approach for such problems, which in principle captures the exact time-evolving density of the physical system via a set of non-interacting Kohn-Sham (KS) orbitals evolving in a one-body potential [1–3]. A key component in this potential is the exchange-correlation potential, $v_{xc}[n; \Psi(0), \Phi(0)](\mathbf{r}, t)$, a functional of the one-body density $n(\mathbf{r}, t' < t)$ (including its past evolution), the interacting initial state $\Psi(0)$ and the choice of initial Kohn-Sham state $\Phi(0)$. This is usually approximated by an adiabatic approximation, within which the instantaneous density is input in a chosen ground-state approximation, $v_{xc}^A[n; \Psi(0), \Phi(0)](\mathbf{r}, t) = v_{xc}^{g.s.}[n(t)](\mathbf{r})$, thus neglecting all the memory-dependence. When orbital-dependent ground-state functionals such as hybrid functionals are used, the corresponding potential depends on the instantaneous orbital, and so has a limited sense of memory. The resulting adiabatic time-dependent Kohn-Sham (TDKS) equations

$$i \partial_t \phi_i(\mathbf{r}, t) = \left[-\frac{1}{2} \nabla^2 + v_s(\mathbf{r}, t) \right] \phi_i(\mathbf{r}, t), \quad (1)$$

with $v_s = v_{\text{ext}} + v_{\text{H}}[n] + v_{xc}^A[n, \Psi(0), \Phi(0)]$ as the sum of the external, Hartree, and adiabatic exchange-correlation potential, have been applied to simulate a range of photo-excited and laser-driven phenomena in molecules and materials at the atto- and femto-

timescales [3–9].

One such domain of application is the use of ultra-short XUV pulses to investigate detailed time-resolved ultrafast dynamics in molecules and clusters, with the promise to reveal the role of correlations and mechanisms in a number of intriguing processes, from Auger decay to charge-migration [10, 11]. A recent series of papers have uncovered an unusual but persistent phenomenon predicted by these simulations [12–16]: a resurgence of a dipole signal some femtoseconds after an ultrafast XUV pulse centered at an off-resonant frequency is turned off. This signal, which has been termed a “dipole-instability”, appears after a period of quiet, almost zero, dipole, that begins to grow with an exponential envelope before reaching a maximum, decaying, and repeating. Such an instability could be measured in principle by time-resolved photo-emission spectroscopy, with a delayed ionization peak corresponding to the resurgence of the dipole. The functional approximation used in the calculations satisfies several exact conditions, including the zero-force theorem, and is energy-conserving, and the dynamics are robust with different choices of numerical parameters. The phenomenon persists across a range of molecules, field strengths, frequencies, and orientations and survives with nuclear motion [13, 14]. The authors have highlighted that the key role of the pulse is in creating a population inversion in the system, and demonstrated that the instability also arises from instead creating an instantaneous hole in a deep-lying state; the dependence on the degree of depletion of this state has also been studied [13, 14, 16]. The population inversion (even partial) has been central in the analyses, where coupling of the upper state to many modes (continuum) is argued to result in a spontaneous symmetry-breaking, backed up by the presence of maxima in phase-space potential energy surfaces near the hole state [16]. While significant insight has been gained, particularly in the drilled hole scenario, the question has remained whether the observed instability is in fact real, or whether it is an

artifact of the approximations inherent in the adiabatic TDKS equations.

Here, we answer this question by considering two different formulations of TDDFT for real-time non-equilibrium dynamics: one is the traditional TDKS approach of Eq. 1, and the other is the recent response-reformulated TDDFT (RR-TDDFT) [17] in which all exchange-correlation quantities needed can be obtained from ground-state or response calculations. While both are exact and would give identical results in the formal case where the exact functionals are used, RR-TDDFT has been demonstrated to be more accurate when the adiabatic approximation is used. Using finite-basis set calculations, we reproduce the instability in the case where it develops after an XUV pulse is applied to the molecule in the TDKS simulation, and we find it is absent in the RR-TDDFT simulation.

We begin in Section II with a recall of the RR-TDDFT approach. In Sec III, we study the dipole dynamics of N_2 , motivated by the case studied in Ref. [13], using both TDKS and RR-TDDFT, keeping all other aspects of the calculation the same as much as possible, i.e. the same functional, the same basis set, and approximately the same treatment of continuum states. Consistently, the TDKS calculation yields the dipole-instability, while RR-TDDFT does not; this holds over a range of different field parameters and classes of functional approximations. We provide an argument for how to understand how the instability observed in the TDKS calculation is onset in Sec. III C. Finally, we conclude in Sec. IV.

II. RESPONSE-REFORMULATED TDDFT

RR-TDDFT proceeds by propagating a set of ordinary differential equations (ODEs) for the coefficients of the time-dependent many-body state expanded in a basis of field-free many-body states $\{\Psi_m\}$, with a key point being that these many-body states are never explicitly constructed [17]. All quantities entering the ODEs can be obtained from ground-state DFT and response TDDFT, and all properties directly related to the density (i.e. representable by one-body multiplicative operators) can in principle be exactly obtained. Like the traditional TDKS formalism, RR-TDDFT is formally exact and its foundation relies on the Runge-Gross theorem [1], which proves a one-to-one mapping between the time-evolving density and a one-body multiplicative external potential. But unlike TDKS, the exchange-correlation terms for RR-TDDFT need to be evaluated only near ground-state densities, not on the fully non-equilibrium density, which makes the approach much more accurate when adiabatic functionals are used.

The time evolution of the expansion coefficients is governed by

$$i\dot{C}_m(t) = E_m C_m(t) + \sum_n V_{mn}^{\text{app}}(t) C_n(t), \quad (2)$$

where the matrix elements of the applied potential are

$$V_{mn}^{\text{app}}(t) = \langle \Psi_m | V^{\text{app}}(t) | \Psi_n \rangle = \int d^3r v^{\text{app}}(\mathbf{r}, t) \rho_{mn}(\mathbf{r}). \quad (3)$$

For the common case of a spatially uniform electric field $\mathcal{E}(t)$, the coupling between the coefficients, Eq. (3), reduces to $V_{mn}^{\text{app}}(t) = \mathcal{E}(t) \cdot \mathbf{d}_{nm}$, with the dipole moment given by

$$\mathbf{d}(t) = \sum_{n,m} C_n^*(t) C_m(t) \mathbf{d}_{nm},$$

where $\mathbf{d}_{nm} = \langle \Psi_n | \hat{\mathbf{r}} | \Psi_m \rangle = \int d^3r \mathbf{r} \rho_{nm}(\mathbf{r})$.

The required inputs for RR-TDDFT are the energies E_m (for $m = 0$ obtained from ground-state DFT and for $m > 0$ from linear-response TDDFT [18–21]), transition densities out of the ground state, $\rho_{0m}(\mathbf{r}) = \langle \Psi_0 | \hat{n}(\mathbf{r}) | \Psi_m \rangle$ (obtained from linear response TDDFT), transition densities between excited states, $\rho_{mn}(\mathbf{r}) = \langle \Psi_m | \hat{n}(\mathbf{r}) | \Psi_n \rangle$ (obtained from quadratic response TDDFT [22, 23]), and state densities $\rho_{mm}(\mathbf{r})$ (for $m = 0$ obtained from ground-state DFT and for $m > 0$ from linear response TDDFT [24–26]). Observables are obtained, in principle [1], from the time-dependent density

$$n(\mathbf{r}, t) = \sum_{n,m} C_n^*(t) C_m(t) \rho_{nm}(\mathbf{r}). \quad (4)$$

For any observable not directly related to the density an additional ‘observable functional’ $O[n, \Psi(0)]$, is needed to extract it from the density and physical initial state. This is similar to the TDKS case, where observables are formally instead functionals of the density and KS initial state.

As mentioned earlier, the advantage of RR-TDDFT over TDKS is that the domain of the needed exchange-correlation functional is far closer to the domain in which they were derived: only ground-state and linear and quadratic response exchange-correlation functionals are needed, not the fully non-equilibrium $v_{\text{xc}}[n; \Psi(0), \Phi(0)](\mathbf{r}, t)$, even though fully non-equilibrium phenomena are being simulated. Making an adiabatic approximation for the latter as in Eq. (1) is clearly a much more drastic approximation for non-equilibrium dynamics than it is for the ground-state and response functionals, since the evaluation of the exchange-correlation term in Eq. (1) is on a density far from the adiabatic regime. As a consequence, as demonstrated in Ref. [17], RR-TDDFT successfully captures phenomena such as Rabi oscillations and charge-transfer dynamics using adiabatic functionals, even in cases where the same approximations fail qualitatively within the TDKS framework. The formalism allows TDDFT to be used with as much reliability and accuracy for non-equilibrium dynamics as it is used in the response regime for spectra. Equally, it is limited by the accuracy of the functional in the response regime, but since the development of improved functionals has

been much more successful for response than for non-equilibrium regime, RR-TDDFT can take advantage of these improvements to describe non-equilibrium dynamics [27].

We note that a similar idea of using TDDFT response quantities in a time-dependent configuration-like framework has been applied to studying electron dynamics in strong fields by a number of groups [28–32], and most recently it has been implemented in an efficient GPU-accelerated code to study dynamics in a large organic molecule (120 atoms) [32]. In those works, only linear response TDDFT quantities and auxiliary wavefunctions were used for the couplings (so relaxation effects for excited-state couplings are missing), and some of these works make a further Tamm-Dancoff-like approximation: RR-TDDFT puts these approximate approaches on a rigorous foundation.

In this paper, we use RR-TDDFT to demonstrate that the unexpected dipole instability observed in the TDKS simulations of Refs. [12–16] is a consequence of the exchange-correlation approximation used, and that it vanishes when the same approximation is used within the RR-TDDFT framework.

III. N₂ DYNAMICS: TDKS VS RR-TDDFT

The simulations of Refs. [12–16] took place in real-space grid codes QDD [33] and EDAMAME [34]. For RR-TDDFT we need quadratic response functionality for the computation of the excited-to-excited state couplings. While linear response TDDFT is available in standard codes, fewer have quadratic response capability, and we are not aware of such a real-space code. We use the finite basis set code turbomole [35] to extract the energies and couplings for RR-TDDFT, and compare with the real-time TDKS evolution performed with NWChem [36] in the same basis set to make a consistent comparison. First we discuss some computational considerations.

A. Computational Details

1. Basis set

We will use the Gaussian basis set cc-pVDZ in all our calculations, except when otherwise noted. The number of many-body states used in the RR-TDDFT calculations shown is 70, however the results are converged with only 40 states for all the cases we consider (this will be explicitly shown later). The excited-to-excited state couplings involve a quadratic response calculation within which the pseudowavefunction approximation was applied to prevent any spurious divergences [37–41].

2. Complex Absorbing Potential

A key consideration in both the real-space simulation of Ref. [13] or our finite-basis set calculation, is the treatment of the ionization continuum: in reality, the part of the electronic wavepacket excited above the ionization threshold will propagate outwards, leaving the system unless driven back by the electric field. To model this ionization, and prevent artificial reflections from boundaries, the real-space grid is typically outfitted with either imaginary potentials or a mask function at the boundaries [13, 42]. With a finite basis-set code, this is more challenging: some approaches use a real-space absorbing potential around each atom [43–45] requiring a large number of diffuse functions in the basis to connect with them, or plane-wave complements are used [46]. A simpler approach was introduced in Ref. [47] where a damping coefficient on molecular orbital energies lying above a threshold is used to mimic the effect of an absorbing potential, and this is implemented in the NWChem software package. Essentially, for the i th orbital energy above a fixed threshold, $\epsilon_i \rightarrow \epsilon_i - i\gamma_i$ where the damping coefficient is defined as:

$$\gamma_i = \gamma_0 [\exp(\xi(\epsilon_i - \epsilon_{th})) - 1], \epsilon_i > \epsilon_{th} \quad (5)$$

where γ_0 is the global damping rate scaling factor, and ξ controls the steepness of the effective complex absorbing potential (CAP) [47]. We set the CAP parameters as: $\gamma_0 = 1\text{H}$, $\xi = 0.5\text{H}^{-1}$ with the threshold energy ϵ_{th} set to zero, and we clamp the upper limit of γ_i to be 100 H. While we do not expect the results from molecular orbital damping applied in this way to correspond exactly to the real-space absorption by a mask or complex boundary, we do expect the effect is similar [47].

To emulate the effect of the CAP within the RR-TDDFT framework, an analogous damping term can instead be introduced at the level of the state amplitudes. In this case, the equations of motion are modified by appending a term of the form $-i\Gamma_m C_m$, on the RHS of Eq. (2) for states with energies above the ionization threshold, in a similar spirit to Eq. (5). However, the parameters used in Eq. (5) would not in general translate over directly, since Eq. (5) applies to molecular orbitals, not to many-body states. For our case, we assume that each TDDFT excitation at an energy above the ionization threshold, is dominated by KS excitations with virtual orbitals at the same or near-lying energies so that using the same parameters could be justified.

3. Linear response spectrum and XUV pulse considerations

Since the details of the electronic structure differ from that used in the real-space grid studies of Refs. [13], the same pulse may lead to different dynamics. Neither the local density approximation with average-density self-interaction correction (ADSIC) functional used in that

work, nor the relaxation-time approximation (RTA) also explored there, are available in the two codes we are using. However, we do not believe the choice of functional is a critical aspect of the phenomenon, as our examples will also explicitly show. Further, Ref. [13] utilized a pseudopotential freezing the cores, while our calculations are all-electron. As much of our analysis will focus on the PBE functional [48] in the cc-pVDZ basis, we show the corresponding spectrum in Figure 1. The stick spectra in both panels indicate the results from frequency-domain matrix equations of linear response, computed in turbomole (essentially the same results as NWChem) with positions at the excitation frequencies and heights determined by the oscillator strength. The smoother filled-in curve shows the results obtained from a real-time calculation of the response, resulting from Fourier-transforming the dipole after a weak δ -kick [49]; no CAP is applied in the top figure which shows good agreement with the stick spectrum from the frequency-domain calculation, with likely increasing agreement and less broadening with increasing duration of the time over which the Fourier transform is taken. The bottom figure applies the CAP, showing the dampening of the oscillator strength above the ionization threshold (computed from the PBE HOMO orbital energy, 9.76 eV).

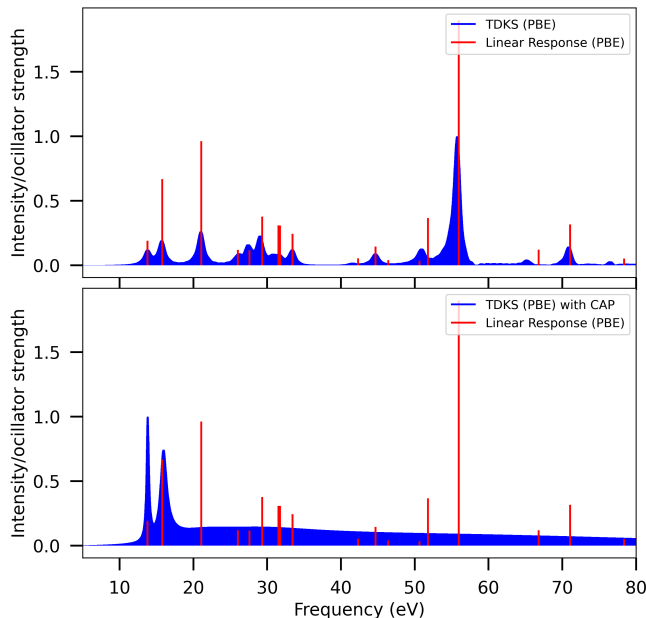


FIG. 1. Comparison of TDDFT (PBE) absorption spectra for N_2 from linear response equations (red stick spectra) and resulting from a kick applied to the TDKS equations (blue filled-in curve); the blue curve is the real-time TDKS intensity normalized to unit maximum, $I_{RT}^{norm}(\omega) = I_{RT}(\omega) / \max_{\omega} I_{RT}(\omega)$, while the red sticks denote the linear-response TDDFT oscillator strengths. The upper panel shows the spectrum obtained from the kick without the CAP applied. The lower panel shows the TDKS spectrum with CAP, with the same linear-response calculation shown for reference.

As expected the lower panel differs in detail from the ADSIC spectrum computed in the real-space basis with absorbing boundaries shown in Fig 1a of Ref. [13], but the trends are similar. In particular, we note that the XUV frequency of $\omega = 58.5\text{eV}$ that was chosen to illustrate the dipole instability in Ref. [13], has the same property of being off-resonant (*c.f.* Figure 1a and 1d of Ref. [13]). It may be useful to note that this frequency lies between the 70th and 71st TDDFT excitation for PBE/cc-pVDZ. Our cases will focus on this frequency as well.

As in Ref. [13], we will apply an ultrafast XUV pulse with the electric field

$$\mathcal{E}(t) = \mathcal{E}_0 \sin^2\left(\frac{\pi t}{T_{\text{pulse}}}\right) \sin(\omega_c t), \quad 0 < t < T_{\text{pulse}} \quad (6)$$

such that $v^{\text{app}}(\mathbf{r}, t) = \mathcal{E}(t)z$ (atomic units are used throughout unless otherwise stated). Ref. [13] chose pulses of duration of 1fs centered in the XUV range, with an intensity such that about 1 electron was absorbed. We will return to the selection of pulse parameters for our study in Sec. III B.

For both the TDKS calculation run in NWChem [36] as well as the RR-TDDFT coefficient evolution run in our in-house code, we use a time step of 0.1 a.u.

4. Computational cost considerations

First, we note that while we do not have a numerically exact electronic structure reference to compare our TDDFT methods against, we will use the approximate coupled-cluster method CC2 as an alternative wavefunction-method reference [50–52], which has often been used to benchmark TDDFT excitation energies [52, 53]. CC2 is an approximation to CCSD, in which singles-dominated excitations are known to well-approximate the CCSD result, while double-excitations are correct only to zeroth order.

Excitation energies and interstate dipole couplings are computed for both CC2 and RR-TDDFT in turbomole, in the cc-pVDZ basis set, with the cost/time for calculation of couplings between excited states from quadratic response scaling far outweighing the linear response. For 40 excited states and their interstate couplings, CC2 required approximately 115 CPU hours. In contrast, the TDDFT/PBE required only 4 CPU hours. This highlights the substantially lower computational scaling of TDDFT-based approaches relative to CC2, particularly as the number of states and couplings increases. In our TDDFT calculations we found that our results were well-converged with 40 states, showing little difference when 80 states were included; going up to 70 states and couplings using TDDFT increased the computational time to 35 CPU hours.

The computational cost/timing of the coefficient evolution for RR-TDDFT or the TDCI/CC2 is negligible compared to the time to obtain the interstate couplings. It is important to note that the expensive part of the

calculation needs to be done only once and for all for a given basis set and functional choice: for the application to dynamics under any field, these same couplings are input and this part of the calculation (propagation of Eqs. (2)) takes a few seconds, involving solving only a system of M ODEs where M is the number of many-body states. In contrast, the TDKS calculation requires solving N non-linear partial differential equations in space and time, with a different calculation for each applied field.

B. N_2 Dipole Instability

We begin by comparing the results of the pulse that was used in Fig. 1d of Ref. [13]. This is: $E_0 = 0.45$ a.u. $= 7 \times 10^{15}$ W/cm², $\omega = 58.5$ eV, and $T_{\text{pulse}} = 1$ fs. Figure 2 shows that the dipole-instability is dramatically evident in our finite-basis TDKS calculation (PBE/cc-pVDZ), occurring in about the same timescale as that in Ref. [13] whose dipole is reproduced in the inset of the top panel. Due to the different functional, basis set, and CAP details, the details are different, and the dipole we obtain is about an order of magnitude greater than that in Ref. [13]. The number of electrons ionized during the pulse is about 1.3, greater than the one electron ionized in Ref. [13].

Turning now to the RR-TDDFT calculation run under the same conditions as our TDKS simulation, we find that the instability is completely absent in RR-TDDFT (shown here including 70 states in the evolution of the coefficients in Eq. (2) but the results are converged using 60 states). This may not be surprising: from the linear structure of the RR-TDDFT equations Eqs. 2, it would be difficult to imagine how the approach would give any change in the magnitude of the dipole oscillations in the absence of any applied field.

Zooming in on earlier times in the lower panel shows that TDKS agrees with RR-TDDFT for the first few cycles, and then differs: the amplitude of the oscillations in TDKS continues to grow until the peak of the applied pulse, while RR-TDDFT peaks earlier and the asymmetry in the fall-off is more significant than in TDKS, with more ionization. We believe this is an inherent difference due to the two different approaches [17, 27] (see also Sec. III C), not a consequence of any choice of numerical parameters. Any limitation in the basis set size affects both calculations. The dipole computed within the larger aug-cc-pVDZ basis set shows only a small difference for the RR-TDDFT and TDKS calculations during the pulse, and the instability in the latter is onset at a slightly larger time but has the same shape and features otherwise (not shown here). However, for the purposes of investigating the dipole instability, these pulse parameters are not ideal for our numerical set-up, since after the pulse is off the oscillations of the dipole never fall below about 0.01 a.u., which is two orders of magnitude larger than the oscillations left in the dipole of

Ref. [13].

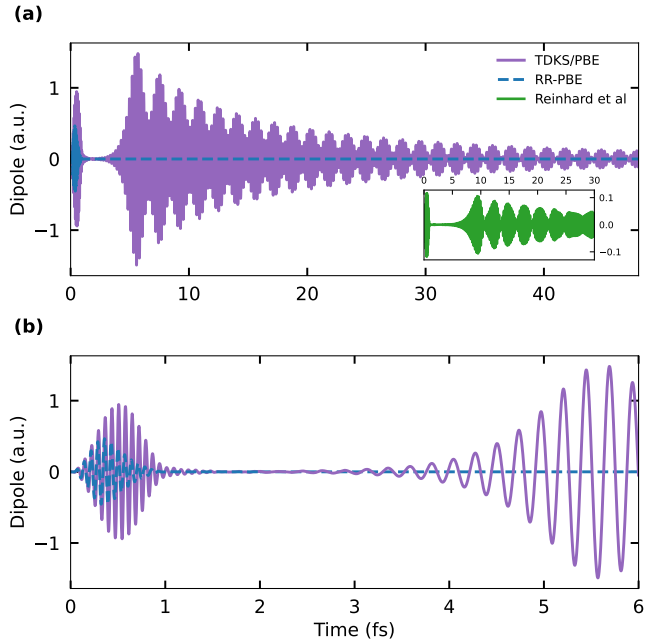


FIG. 2. Time-dependent dipole of N_2 computed using TDKS and RR-TDDFT approaches under the applied field ($E_0 = 0.45$ a.u., $\omega = 58.5$ eV, $T_{\text{pulse}} = 1$ fs in Eq. 6), both within PBE/cc-pVDZ. **Top panel:** TDKS (purple, solid) and RR-TDDFT (blue, dashed) predictions using 70 states. Couplings between excited states in RR-TDDFT were computed within the pseudowavefunction approximation, and both calculations used the effective CAPs described in the text. The inset shows the results from Ref. [13], computed from TDKS within LDA-ADSIC in a real-space grid with a mask function absorbing boundary. **Bottom panel:** As in the top panel but zoomed into the early-time regime (0–6 fs).

We therefore focus on a weaker pulse with parameters $E_0 = 0.15$ a.u., $\omega = 58.5$ eV, and $T_{\text{pulse}} = 2$ fs. Figure 3 shows the dipole resulting from the TDKS and RR-TDDFT calculations, both again using the PBE functional in the cc-pVDZ basis. After a longer quiet initial post-pulse behavior, the dipole-instability in the TDKS evolution is again evident, and completely absent in the RR-TDDFT approach. The middle panel shows that during the pulse, the two methods give similar results, practically matching during the first five or so cycles, and remaining in phase throughout, with TDKS climbing to larger oscillation amplitudes towards the second half of the pulse. With the chosen CAP 0.38 electrons are ionized after the pulse in the TDKS calculation before the onset of the dipole resurgence, while 4.5 are ionized in the RR-TDDFT calculation. The RR-TDDFT dipole matches very closely with the TD-CI approach using CC2 energies and couplings as input, both during the pulse and in their absence of instability; using the same CAP function as in the RR-TDDFT calculation produces an ionization yield of 1.84 electrons in the CC2 calculation. Again, we believe the salient difference observed

between the TDKS and RR-TDDFT calculations (different ionization yields and, especially, instability behavior) is inherent to the methods themselves rather than being a consequence of numerical parameters. At the same time, it should be noted that to understand quantitative differences in the dynamics during the pulse and the ionization yields, a deeper investigation of what the equivalent CAP should be between the two methods would be needed.

The bottom panel of Fig. 3 shows the RR-TDDFT dipole computed using different numbers of states and their couplings, showing that the dipole converges with about 40 states included. To confirm that the basis set

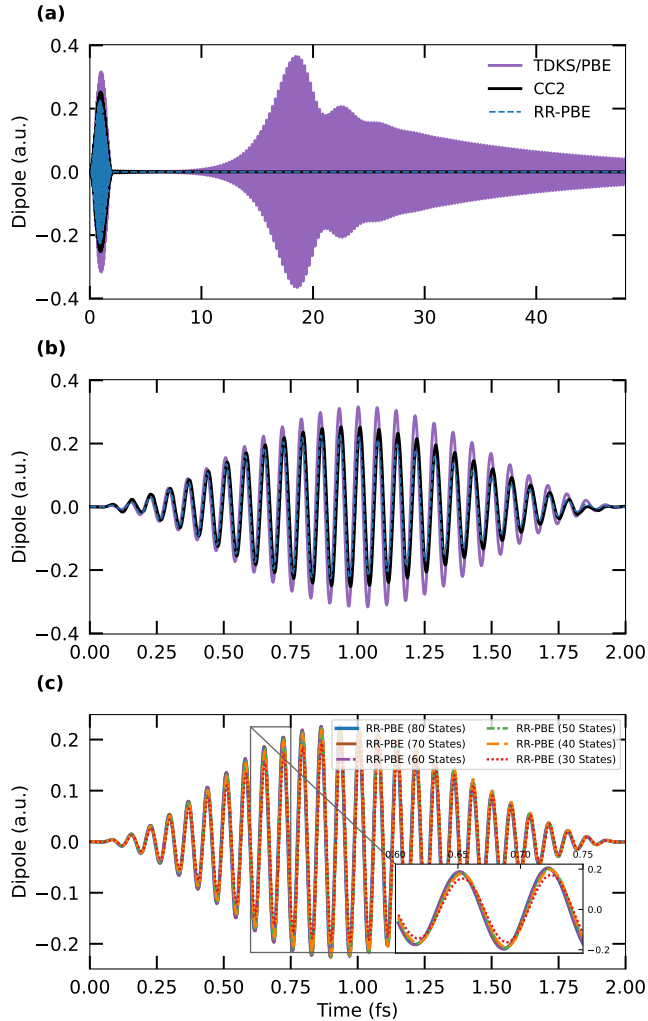


FIG. 3. Time-dependent dipole dynamics computed using time-dependent TDKS, RR-TDDFT, and CC2 approaches under the applied field ($E_0 = 0.15$ a.u., $\omega = 58.5$ eV, $T_{\text{pulse}} = 2$ fs). **Top panel:** TDKS and RR-TDDFT dipoles with the PBE functional (cc-pVDZ) and CC2 using 40 states. **Middle panel:** The dipoles shown during the pulse. All simulations include the CAP described in the text. **Bottom panel:** Convergence of the RR-TDDFT dynamics as a function of the number of states.

choice is not a critical factor in the phenomenon, we

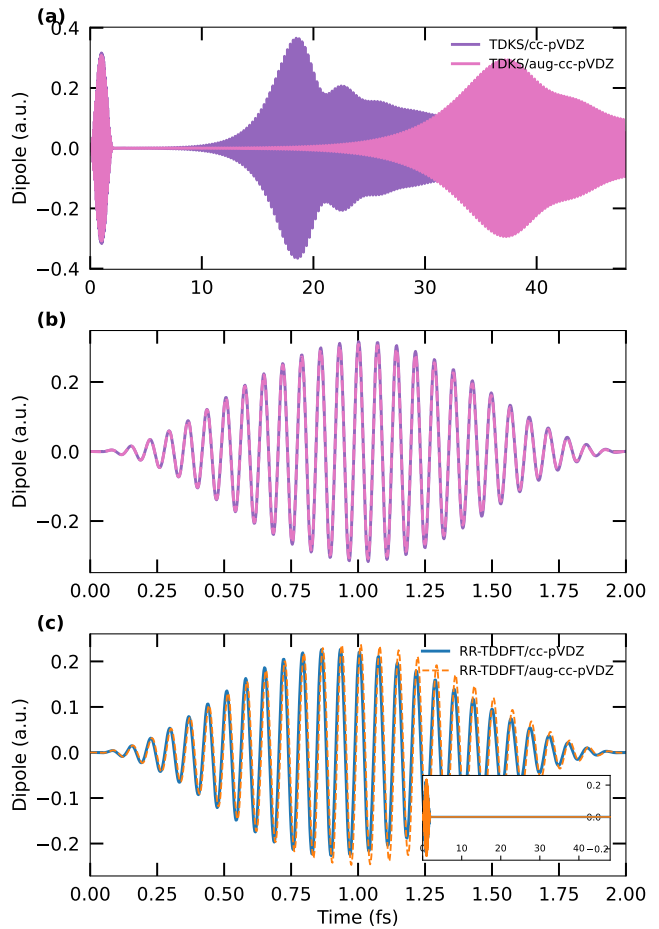


FIG. 4. Time-dependent dipole dynamics illustrating basis set dependence on TDKS and RR-TDDFT approaches under the applied field ($E_0 = 0.45$ a.u., $\omega = 58.5$ eV, $T_{\text{pulse}} = 2$ fs). **Top panel:** TDKS/PBE with cc-pVDZ and aug-cc-pVDZ basis sets. **Middle panel:** As in top panel but zoomed in for times during the pulse. **Bottom panel:** RR-TDDFT/PBE with energies and couplings computed in cc-pVDZ and aug-cc-pVDZ as indicated. The inset shows the corresponding evolution over a longer time range.

compare the dipoles using the aug-cc-pVDZ basis in Figure 4. The top panel shows that the instability remains in the larger basis set, albeit delayed and we note that the ionization yield reduces slightly to 0.368 electrons during the pulse. The middle panel shows that during the pulse there is almost no difference in the dipole dynamics. Again, RR-TDDFT shows no instability, as shown in the bottom panel, and there is a small difference in the oscillations during the pulse, with the ionization yield after the pulse reducing to 2.78 electrons.

Figure 5 shows the TDKS and RR-TDDFT dipole dynamics for a range of field-strengths. The larger the field strength, the faster and larger the onset of the dipole resurgence for this range of intensities; note that while on the scale of the initial dipole driven by the field, the

instability is barely visible for the weakest field shown ($E_0/5$) but zooming in shows it is there (see inset in the upper panel). In all cases there is no growth whatsoever in any of the RR-TDDFT results; as noted earlier, the linear nature of Eqs. (2) preclude such a growth in the absence of the field.

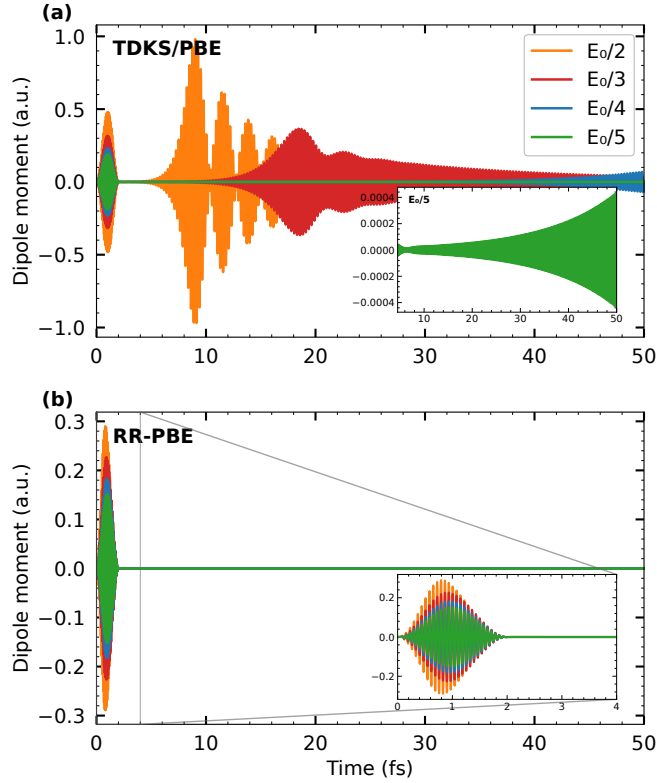


FIG. 5. Time-dependent dipole moment under the 2fs, $\omega_c = 58.5\text{eV}$ pulse with varying pulse strengths: $E_0/2$ (orange), $E_0/3$ (red), $E_0/4$ (blue), and $E_0/5$ (green), where $E_0 = 0.45\text{ a.u.}$: (a) TDKS/PBE and (b) RR-PBE.

C. Towards understanding the dipole-instability of TDKS

These results show that using the PBE functional within TDKS gives the dipole-instability while PBE used within RR-TDDFT does not. This is not a feature particular to the PBE exchange-correlation functional (nor the LDA-ADSIC or RTA explored in Refs. [12–16]), but applies to many classes of functional approximations. We show this in Figure 6, where in contrast to the GGA class of functional (PBE), we show a hybrid (PBE0) [54], a meta-GGA ($r^2\text{SCAN}$) [55, 56], and the self-interaction free correlation-less time-dependent Hartree-Fock (TDHF) [57]. The onset and other details of the post-pulse dipole-instability can differ significantly depending on the functional. For example, for TDHF, the onset is much slower such that the same oscillation amplitudes are reached hundreds of femtoseconds later than for PBE, PBE0, or $r^2\text{SCAN}$. For a more

intense pulse of amplitude three times that shown here, the maximum of the first dipole resurgence is reached at around 175 fs in TDHF, but around 5fs in PBE. This implies that self-interaction may play a key role in the instability, but while a self-interaction-free functional delays the onset, it does not eliminate it. We also note the ionization yields during the pulses differ depending on the functional: within TDKS the ionization yields were 0.338, 0.397, and 0.273 electrons for PBE0, $r^2\text{SCAN}$, and TDHF respectively, while larger (4.9, 5.6, and 4.45) respectively for RR-TDDFT. Although not shown here, if we adjust the CAP so as to get a similar ionization yield from RR-TDDFT than for the TDKS, RR-TDDFT still does not produce the dipole-instability. As noted in Refs. [13, 15], the appearance or absence of the instability also depends on the frequency of the pulse; this is true also for the finite-basis case (although again not shown here).

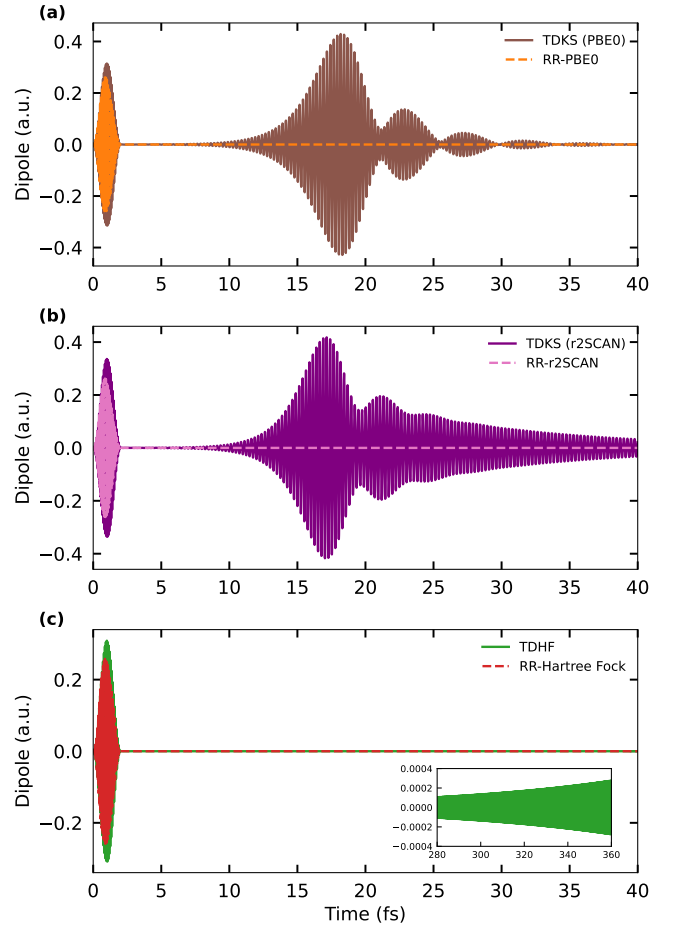


FIG. 6. Dipole instability in TDKS under different functional approximations, compared against RR-TDDFT with the same functional. **Top panel:** Hybrid functional PBE0 **Middle panel:** Meta-GGA functional $r^2\text{SCAN}$. **Bottom panel:** Hartree-Fock. Note the different timescales in each of the panels.

In all cases, there is no dipole-instability in RR-TDDFT: In the absence of a field, only the free-evolution

term of Eqs. (2) (first term) is active, and the magnitude of the coefficients remains the same as they were when the field is turned off, except for the exponential decay the CAP causes. In fact, the molecule returns primarily back in the ground-state after the pulse; due to the off-resonant nature, even during the pulse only a small fraction (maximum 2.54%) of the electron density enters the excited states as shown in Fig. 7. The linear structure of the ODEs ensures not only a stable propagation but also makes it impossible for exponential growth to occur without a field present. While the separation of spatial- and time-dependence was noted to be advantageous from the point of view of exchange-correlation functional dependence in Ref. [17], here we see another advantage is the removal of unphysical behavior arising from incorrect non-linearity.

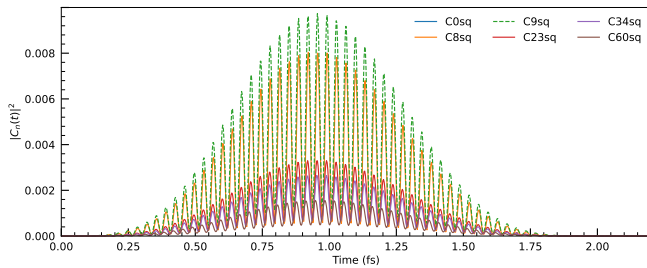


FIG. 7. Time-dependent evolution of the largest excited-state populations ($|C_N|^2$) obtained from the RR-TDDFT simulation under an applied field ($E_0 = 0.15$, $\omega = 58.5$ eV, $T_{\text{pulse}} = 2$ fs). Only states with a maximum population exceeding 10^{-3} are shown. The population dynamics exhibit coherent buildup and decay within the pulse envelope, with a small subset of states dominating the excitation manifold.

To try to understand how the dipole instability emerges in the TDKS system, consider the initial behavior of the dipole after the pulse is off. The top panel of Figure 8 shows that consists of very small oscillations of frequency about 16 eV in *all* cases where instability occurs, regardless of pulse parameters, which corresponds to about the 8th excitation (the second noticeable peak in the spectrum) for each of the functionals. Given the off-resonant nature of the pulse and the coefficients in RR-TDDFT, we expect that even in TDKS, the system returns largely to the ground-state after the pulse. We assert that during the initial period after the pulse is turned off, the density has the form:

$$n(\mathbf{r}, t) = \mathcal{N}(n_0(\mathbf{r}) + \delta(t) \sin(\Omega_n t) n^{(1)}(\mathbf{r}) + O(\delta^2)) \quad (7)$$

where $\delta(t)$ is a small amplitude which varies in time more slowly than the frequency of oscillations $\Omega_n \approx 16 \text{ eV} \approx E_8 - E_0$, and $n_0(\mathbf{r})$ indicates the ground-state density. For example, this form would arise if one (or more) of the TDKS orbitals after the pulse was left in the superposition $\phi_{\text{occ}}(\mathbf{r}) + \delta(0)\phi_8(\mathbf{r})$, such that its density is $|\phi_{\text{occ}}(\mathbf{r})|^2 + 2\text{Re}(\delta(0)\phi_{\text{occ}}(\mathbf{r})\phi_8(\mathbf{r}))$ to $O(\delta)$, in which case the normalization factor $\mathcal{N} = 1$ to linear order in δ ,

because the transition-density integrates to zero. Evaluating the time-dependent Hartree-exchange-correlation potential, $v_{\text{HXC}} = v_{\text{H}} + v_{\text{XC}}$, on the density of Eq. (7) and expanding up to $O(\delta)$ we have:

$$v_{\text{HXC}}^{\text{adia}}[n](\mathbf{r}, t) = v_{\text{HXC}}^{\text{adia}}[n_0](\mathbf{r}) + \underbrace{\int f_{\text{HXC}}^{\text{adia}}[n_0](\mathbf{r}, \mathbf{r}') n^{(1)}(\mathbf{r}') d^3 r'}_{= C(\mathbf{r})} \cdot \delta(t) \sin(\Omega_n t) \quad (8)$$

This means that the TDKS Hamiltonian driving the orbitals is, to $O(\delta)$,

$$h_{\text{S}} = h_{\text{S}}^{(0)} + 2\delta(t)C(\mathbf{r}) \sin(\Omega_n t) \quad (9)$$

That is, the TDKS system is driven by the field-free ground-state KS Hamiltonian plus a small driving term that is resonant with one of the linear-response frequencies of the system. When any system is driven at its resonant frequency the oscillations grow, i.e. $\delta(t)$ will get larger until the perturbation approximation is no longer valid. But at that time, the larger changes in the density lead to the resonant frequencies of the TDKS system beginning to change significantly, as has been discussed in the literature as the spurious peak-shifting problem of adiabatic TDDFT [58–60], so that the growth of the oscillations peaks and then falls.

A key point in the above argument is the dependence of the functional in Eq. (8) on the instantaneous density. It is not the non-linearity *per se* of the functional, but rather the instantaneous dependence. The artificial self-driving effect would not arise with an appropriate memory-dependent functional (also nonlinear), as in the case of the exact functional, because such a functional would not be perfectly in sync with the density oscillations; the term $C(\mathbf{r})$ in Eq. (8) would be time-dependent. The argument also rests on the assumption that the system is left with very small (pure or commensurate) oscillations after the pulse, and suggests that any time this happens there will be a tendency towards an exponential growth of these oscillations with an adiabatic functional i.e. the dipole-instability. The argument highlights the crucial role of the CAP: without the CAP, the system is left oscillating with a wider, more noisy, spectrum of frequencies after the pulse, between which interference effects prevent the self-driving effect to occur. Indeed, the dipole-instability vanishes in all cases when the CAP is turned off; an example is shown in Fig. 8b. The CAP has less of a significant role in RR-TDDFT: other than the small post-pulse oscillations and larger signal during the pulse that occur when the CAP is removed, the results are qualitatively similar with and without it, as shown in Fig. 8c. With the CAP on, we have found that in cases where the dipole-instability does not arise (not shown here), the system appears to be left oscillating in a more complex way with more frequencies. Our argument does not address *when* we can predict the system is left with essentially one (or a few

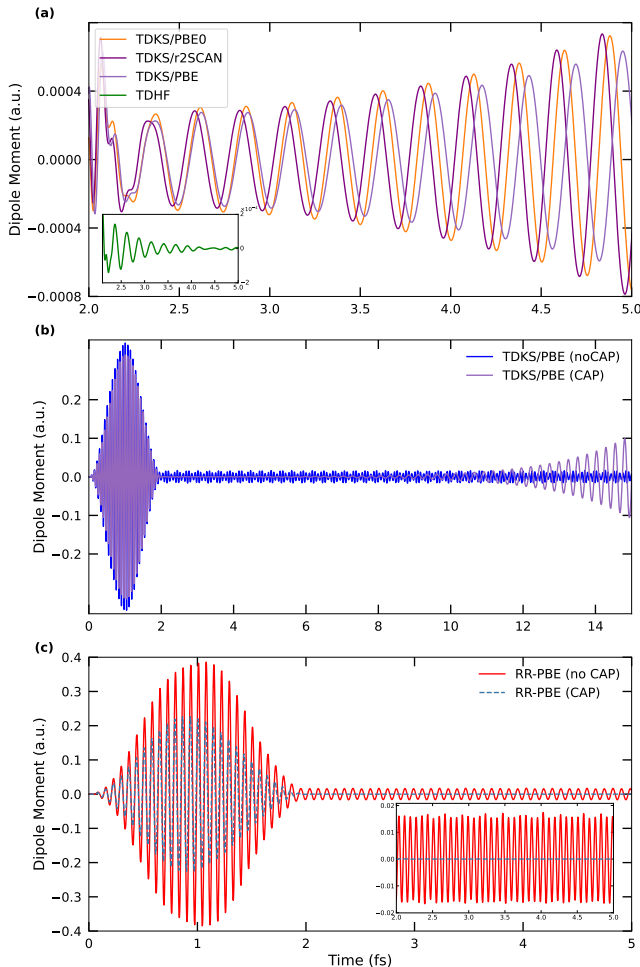


FIG. 8. Time-dependent dipole dynamics computed using TDKS and RR-TDDFT approaches under the applied field ($E_0 = 0.15$ a.u., $\omega = 58.5$ eV, $T_{\text{pulse}} = 2$ fs). **Top panel:** Zoomed view of the TDKS dipole evolution shortly after the pulse, with PBE, PBE0, r^2 SCAN functionals, all with CAP applied. The inset shows the TDHF dipole over the same window. The oscillation frequency observed in the 2–5 fs window for each functional corresponds to its respective 8th excitation frequency: 0.0922 a.u. (TDHF), 0.0922 a.u. (PBE), 0.0922 a.u. (PBE0), and 0.0943 a.u. (r^2 SCAN). The corresponding oscillation periods are approximately 0.2624 fs (TDHF), 0.2624 fs (PBE), 0.2624 fs (PBE0), and 0.2565 fs (r^2 SCAN). **Middle panel:** Comparison of the TDKS/PBE dipole with and without CAP applied. **Bottom panel:** RR-TDDFT/PBE dipole dynamics with and without CAP during the pulse and shortly after. The inset shows a zoomed view between 2 and 5 fs.

commensurate) frequencies after the pulse, and a more complete investigation is left for future work.

IV. CONCLUSIONS AND OUTLOOK

While the adiabatic approximation in TDKS has produced useful results in many cases, and in particular has enabled the study of electron dynamics in systems too

large to be studied otherwise, e.g. Refs. [4–7, 61, 62], the lack of memory-dependence has also been found to be the root of large errors, unreliable results, and failures [9, 63–72]. The present numerical results and analysis suggest that the post-pulse dipole instability discovered in recent works [12–16] represents another case where the lack of memory-dependence gives qualitatively wrong behavior. The instantaneous dependence on the density leads to an incorrect non-linearity in the TDKS Hartree-exchange-correlation potential that self-drives small almost pure oscillations in the system after the pulse, until the oscillations grow so as to detune itself through spurious peak-shifting. The CAP plays a critical role: turning it off means that the system is left in a more ‘noisy’ state, with different frequencies interfering such that the artificial resonant effect does not occur.

This unphysical behavior vanishes when the very same approximation is used in RR-TDDFT. Exponential growth is not possible within the linear ODE structure of the time-evolution equations in the absence of any field. This example then highlights another advantage of separating out the space and time dependence in TDDFT as RR-TDDFT does: while Ref. [17] noted this reduces the complexity arising from the inherent weaving of space and time non-localities in the full v_{xc} functional, we note here that it also removes unphysical behavior arising from the incorrect non-linear dependence of adiabatic functional approximations.

Throughout the dynamics, the closer agreement with CC2 of RR-TDDFT over TDKS using any of the functionals studied here is consistent with our expectation that even aside from the instability question, the RR-TDDFT framework is more accurate than TDKS with adiabatic functionals because these functionals are evaluated on a domain close to the domain in which they were derived. These functionals miss states of double-excitations, while CC2 contains them although in an approximate way, so this could be part of the difference in their predictions of the dynamics. While TDKS can access states these states, it does so in an unreliable and inconsistent way [27, 73].

Further, we believe that the question of double-excitations is related to divergences that appear in excited-to-excited state couplings from quadratic response TDDFT and CC2 [37, 41, 74]; the pseudowavefunction approximation we used in the TDDFT couplings avoids these unphysical divergences. However, we found that they did not influence the dynamics of the dipole significantly in the cases studied in this paper: both full quadratic response and even an unrelaxed calculation of the couplings gave similar results for the dipole-dynamics in these cases, suggesting it is likely that within the functionals used, such states were not significantly involved in the dynamics, or at least did not affect the dipole observable much.

While the results here unequivocally demonstrate that the dipole instability of TDKS vanishes when the same functional is used within RR-TDDFT, the quanti-

tative difference in their predictions while the pulse is on needs further investigation. In particular, a more careful analysis of how a particular CAP used on the molecular orbitals in TDKS should translate over to the CAP on the underlying many-body states in RR-TDDFT is needed and left for future work. Also left for future work is a deeper analysis beyond that given in Sec. III C on the self-driving resonance effect that we believe is at the root of the instability in adiabatic TDKS, including understanding details such as how the onset times depend on the functional as well as on predicting field parameters for which the instability occurs or not. Finally, the cases studied here do not model the case where the system begins in an excited cationic state as was a focus in Refs. [12, 14, 16]; what we can learn from comparing RR-TDDFT and TDKS dynamics starting in such a ‘drilled hole’ state will be a future study.

ACKNOWLEDGMENTS

We thank Phuong Mai Dinh, Paul-Gerhard Reinhard, Eric Suraud, and Tchavdar Todorov, for lively and stimulating discussions about the dipole instability. Financial support from the National Science Foundation Award CHE-2154829 (DR) and the Department of Energy, Office of Basic Energy Sciences, Division of Chemical Sciences, Geosciences and Biosciences under Award No. DE-SC0024496 (NTM) are gratefully acknowledged. The authors acknowledge the Office of Advanced Research Computing (OARC) at Rutgers, The State University of New Jersey for providing access to the Amarel cluster and associated research computing resources that have contributed to the results reported here.

-
- [1] E. Runge and E. K. U. Gross, Density-functional theory for time-dependent systems, *Phys. Rev. Lett.* **52**, 997 (1984).
- [2] C. A. Ullrich, *Time-dependent density-functional theory: concepts and applications* (Oxford University Press, 2011).
- [3] N. T. Maitra, Perspective: Fundamental aspects of time-dependent density functional theory, *The Journal of Chemical Physics* **144**, 220901 (2016), <https://doi.org/10.1063/1.4953039>.
- [4] X. Li, N. Govind, C. Isborn, A. E. DePrince III, and K. Lopata, Real-time time-dependent electronic structure theory, *Chem. Rev.* **120**, 9951 (2020), pMID: 32813506.
- [5] S. A. Sato, First-principles calculations for attosecond electron dynamics in solids, *Computational Materials Science* **194**, 110274 (2021).
- [6] C. Shepard, R. Zhou, D. C. Yost, Y. Yao, and Y. Kanai, Simulating electronic excitation and dynamics with real-time propagation approach to tddft within plane-wave pseudopotential formulation, *J. Chem. Phys.* **155**, 100901 (2021), <https://doi.org/10.1063/5.0057587>.
- [7] L. Bhan, C. Covington, and K. Varga, Signatures of atomic structure in subfemtosecond laser-driven electron dynamics in nanogaps, *Phys. Rev. B* **105**, 085416 (2022).
- [8] C. A. Ullrich, A snapshot of time-dependent density-functional theory, *APL Computational Physics* **1**, 020901 (2025).
- [9] L. Lacombe and N. T. Maitra, Non-adiabatic approximations in time-dependent density functional theory: progress and prospects, *npj Comput. Mater.* **9**, 124 (2023).
- [10] M. F. Ciappina, J. A. Perez-Hernandez, A. S. Landsman, W. A. Okell, S. Zherebtsov, B. Förg, J. Schötz, L. Seifert, T. Fennel, T. Shaaran, T. Zimmermann, A. Chacon, R. Guichard, A. Zaïr, J. W. G. Tisch, J. P. Marangos, T. Witting, A. Braun, S. A. Maier, L. Roso, M. Krüger, P. Hommelhoff, M. F. Kling, F. Krausz, and M. Lewenstein, Attosecond physics at the nanoscale, *Rep. Prog. Phys.* **80**, 054401 (2017).
- [11] L. Young, K. Ueda, M. Gühr, P. H. Bucksbaum, M. Simon, S. Mukamel, N. Rohringer, K. C. Prince, C. Masciovecchio, M. Meyer, A. Rudenko, D. Rolles, C. Bostedt, M. Fuchs, D. A. Graves, J. Krzywinski, D. A. Reis, B. Rudek, B. Erk, R. Coffee, S. L. König, T. Fehenberger, S. H. Southworth, L. F. DiMauro, P. Salen, P. vander Meulen, H. T. Muhammed, J. Larsson, M. Richardson, R. Moshhammer, J. Ullrich, M. Martins, A. Knie, A. Rouzee, A. Hundertmark, M. Simon, M. Vrakking, T. M. Baumann, R. Boll, C. Bomme, B. Erk, E. Saveljev, N. Schirmel, S. Techert, and D. Rolles, Roadmap of ultrafast x-ray atomic and molecular physics, *J. Phys. B: At. Mol. Opt. Phys.* **51**, 032003 (2018).
- [12] P.-G. Reinhard, P. M. Dinh, D. Dundas, E. Suraud, and M. Vincendon, On the stability of hole states in molecules and clusters, *Eur. Phys. J. Spec. Top.* **232**, 2095 (2023).
- [13] P.-G. Reinhard, D. Dundas, P. M. Dinh, M. Vincendon, and E. Suraud, Unexpected dipole instabilities in small molecules after ultrafast xuv irradiation, *Physical Review A* **107**, L020801 (2023).
- [14] D. Hughes, D. Dundas, P. M. Dinh, M. Vincendon, P.-G. Reinhard, and E. Suraud, Dipole instability in molecules irradiated by XUV pulses, *The European Physical Journal D* **77**, 177 (2023).
- [15] D. Hughes, D. Dundas, P. M. Dinh, E. Suraud, and P.-G. Reinhard, Dipole instability after an ultrashort xuv pulse in n2: population inversion and timescales, *Scientific Reports* **15**, 43692 (2025).
- [16] P. M. Dinh, P.-G. Reinhard, D. Dundas, D. Hughes, and E. Suraud, Symmetry breaking in TDLDA dynamics of symmetric molecules, *Eur. Phys. J. D* (2026), in press.
- [17] D. B. Dar, A. Baranova, and N. T. Maitra, Reformulation of time-dependent density functional theory for nonperturbative dynamics: The rabi oscillation problem resolved, *Phys. Rev. Lett.* **133**, 096401 (2024).
- [18] M. Petersilka, U. J. Gossmann, and E. K. U. Gross, Excitation energies from time-dependent density-functional theory, *Phys. Rev. Lett.* **76**, 1212 (1996).
- [19] M. Casida, Time-dependent density functional response theory for molecules, in *Recent Advances in Density Functional Methods, Part I*, edited by D. Chong (World Scientific, Singapore, 1995).
- [20] M. E. Casida, Time-dependent density functional response theory of molecular systems: Theory, computational methods, and functionals, in *Recent Developments and Applications of Modern Density Functional Theory*,

- edited by J. M. Seminario (Elsevier, Amsterdam, 1996) p. 391.
- [21] T. Grabo, M. Petersilka, and E. Gross, Molecular excitation energies from time-dependent density functional theory, *Journal of Molecular Structure: THEOCHEM* **501**, 353 (2000).
- [22] S. M. Parker and F. Furche, Response theory and molecular properties, in *Frontiers of Quantum Chemistry*, edited by M. J. Wójcik, H. Nakatsuji, B. Kirtman, and Y. Ozaki (Springer Singapore, Singapore, 2018) pp. 69–86.
- [23] P. Salek, O. Vahtras, T. Helgaker, and H. Ågren, Density-functional theory of linear and nonlinear time-dependent molecular properties, *The Journal of Chemical Physics* **117**, 9630 (2002), https://pubs.aip.org/aip/jcp/article-pdf/117/21/9630/19225236/9630.1_online.pdf.
- [24] F. Furche, On the density matrix based approach to time-dependent density functional response theory, *The Journal of Chemical Physics* **114**, 5982 (2001).
- [25] F. Furche and R. Ahlrichs, Adiabatic time-dependent density functional methods for excited state properties, *The Journal of Chemical Physics* **117**, 7433 (2002).
- [26] A. Baranova and N. T. Maitra, Excited-State Densities from Time-Dependent Density Functional Response Theory, *Journal of Chemical Theory and Computation* **10.1021/acs.jctc.5c00909** (2025).
- [27] D. Ray, A. Baranova, D. B. Dar, and N. T. Maitra, Harnessing dressed time-dependent density functional theory for the nonperturbative regime: Electron dynamics with double excitations, *APS Open Sci.* **1**, L000014 (2026).
- [28] J. A. Sonk and H. B. Schlegel, TD-CI Simulation of the Electronic Optical Response of Molecules in Intense Fields II: Comparison of DFT Functionals and EOM-CCSD, *The Journal of Physical Chemistry A* **115**, 11832 (2011).
- [29] B. Mignolet, R. D. Levine, and F. Remacle, Charge migration in the bifunctional PENNA cation induced and probed by ultrafast ionization: A dynamical study, *Journal of Physics B: Atomic, Molecular and Optical Physics* **47**, 124011 (2014).
- [30] G. Hermann, V. Pohl, and J. C. Tremblay, An open-source framework for analyzing N-electron dynamics. II. hybrid density functional theory/Configuration Interaction methodology, *J. Comput. Chem.* **38**, 2378 (2017).
- [31] E. Coccia and E. Luppi, Time-dependent ab initio approaches for high-harmonic generation spectroscopy, *Journal of Physics: Condensed Matter* **34**, 073001 (2021).
- [32] T. Knoll and B. G. Levine, Simulating electron dynamics with gpu-accelerated real-time tamm-dancoff approximation, *Journal of Chemical Theory and Computation* **0**, null (0), <https://doi.org/10.1021/acs.jctc.6c00129>.
- [33] P. Dinh, M. Vincendon, F. Coppens, E. Suraud, and P.-G. Reinhard, Quantum dissipative dynamics (qdd): A real-time real-space approach to far-off-equilibrium dynamics in finite electron systems, *Computer Physics Communications* **270**, 108155 (2022).
- [34] D. Dundas, Multielectron effects in high harmonic generation in n2 and benzene: Simulation using a non-adiabatic quantum molecular dynamics approach for laser-molecule interactions, *The Journal of Chemical Physics* **136**, 194303 (2012).
- [35] TURBOMOLE V7.2 2017, a development of University of Karlsruhe and Forschungszentrum Karlsruhe GmbH, 1989-2007, TURBOMOLE GmbH, since 2007; available from <http://www.turbomole.com> (2017).
- [36] M. Valiev, E. Bylaska, N. Govind, K. Kowalski, T. Straatsma, H. V. Dam, D. Wang, J. Nieplocha, E. Apra, T. Windus, and W. de Jong, Nwchem: A comprehensive and scalable open-source solution for large scale molecular simulations, *Computer Physics Communications* **181**, 1477 (2010).
- [37] S. M. Parker, S. Roy, and F. Furche, Unphysical divergences in response theory, *The Journal of Chemical Physics* **145**, 134105 (2016), <http://dx.doi.org/10.1063/1.4963749>.
- [38] Z. Li and W. Liu, First-order nonadiabatic coupling matrix elements between excited states: A lagrangian formulation at the cis, rpa, td-hf, and td-dft levels, *The Journal of Chemical Physics* **141**, 014110 (2014).
- [39] Q. Ou, G. D. Bellchambers, F. Furche, and J. E. Subotnik, First-order derivative couplings between excited states from adiabatic TDDFT response theory, *J. Chem. Phys.* **142**, 064114 (2015).
- [40] X. Zhang and J. M. Herbert, Analytic derivative couplings in time-dependent density functional theory: Quadratic response theory versus pseudo-wavefunction approach, *J. Chem. Phys.* **142**, 064109 (2015).
- [41] S. M. Parker, D. Rappoport, and F. Furche, Quadratic response properties from tddft: Trials and tribulations, *Journal of chemical theory and computation* **14**, 807 (2018).
- [42] P.-G. Reinhard, P. D. Stevenson, D. Almehe, J. A. Maruhn, and M. R. Strayer, Role of boundary conditions in dynamic studies of nuclear giant resonances and collisions, *Phys. Rev. E* **73**, 036709 (2006).
- [43] P. Krause, J. A. Sonk, and H. B. Schlegel, Strong field ionization rates simulated with time-dependent configuration interaction and an absorbing potential, *The Journal of Chemical Physics* **140**, 174113 (2014).
- [44] A. Sissay, P. Abanador, F. Mauger, M. Gaarde, K. J. Schafer, and K. Lopata, Angle-dependent strong-field molecular ionization rates with tuned range-separated time-dependent density functional theory, *The Journal of Chemical Physics* **145**, 094105 (2016).
- [45] A. S. Durden and H. B. Schlegel, Evaluation of diffuse basis sets for simulations of strong field ionization using time-dependent configuration interaction with a complex absorbing potential, *J. Phys. Chem. A* **129**, 3353 (2025).
- [46] B. Mignolet, R. D. Levine, and F. Remacle, Localized electron dynamics in attosecond-pulse-excited molecular systems: Probing the time-dependent electron density by sudden photoionization, *Phys. Rev. A* **86**, 053429 (2012).
- [47] K. Lopata and N. Govind, Near and above ionization electronic excitations with non-hermitian real-time time-dependent density functional theory, *Journal of Chemical Theory and Computation* **9**, 4939 (2013), pMID: 26583412, <https://doi.org/10.1021/ct400569s>.
- [48] J. P. Perdew, K. Burke, and M. Ernzerhof, Generalized gradient approximation made simple, *Phys. Rev. Lett.* **77**, 3865 (1996).
- [49] K. Yabana, T. Nakatsukasa, J.-I. Iwata, and G. Bertsch, Real-time, real-space implementation of the linear response time-dependent density-functional theory, *Physica Status Solidi (b)* **243**, 1121 (2006).
- [50] O. Christiansen, H. Koch, and P. Jørgensen, The second-order approximate coupled cluster singles and doubles model cc2, *Chemical Physics Letters* **243**, 409 (1995).
- [51] K. Hald, C. Hättig, D. L. Yeager, and P. Jørgensen, Linear response cc2 triplet excitation energies, *Chemical Physics*

- Letters **328**, 291 (2000).
- [52] M. R. Silva-Junior, M. Schreiber, S. P. A. Sauer, and W. Thiel, Benchmarks for electronically excited states: Time-dependent density functional theory and density functional theory based multireference configuration interaction, *The Journal of Chemical Physics* **129**, 104103 (2008), https://pubs.aip.org/aip/jcp/article-pdf/doi/10.1063/1.2973541/11068680/104103.1_online.pdf.
- [53] A. D. Laurent and D. Jacquemin, Td-dft benchmarks: A review, *International Journal of Quantum Chemistry* **113**, 2019 (2013), <https://onlinelibrary.wiley.com/doi/pdf/10.1002/qua.24438>.
- [54] C. Adamo and V. Barone, Toward reliable density functional methods without adjustable parameters: The pbe0 model, *The Journal of Chemical Physics* **110**, 6158 (1999).
- [55] J. Sun, A. Ruzsinszky, and J. P. Perdew, Strongly constrained and appropriately normed semilocal density functional, *Phys. Rev. Lett.* **115**, 036402 (2015).
- [56] J. W. Furness, A. D. Kaplan, J. Ning, J. P. Perdew, and J. Sun, Accurate and numerically efficient r2scan meta-generalized gradient approximation, *The Journal of Physical Chemistry Letters* **11**, 8208 (2020), pMID: 32876454, <https://doi.org/10.1021/acs.jpcllett.0c02405>.
- [57] A. D. McLACHLAN and M. A. BALL, Time-dependent hartree-fock theory for molecules, *Rev. Mod. Phys.* **36**, 844 (1964).
- [58] J. I. Fuks, N. Helbig, I. Tokatly, and A. Rubio, Non-linear phenomena in time-dependent density-functional theory: What rabi oscillations can teach us, *Phys. Rev. B* **84**, 075107 (2011).
- [59] J. I. Fuks, K. Luo, E. D. Sandoval, and N. T. Maitra, Time-resolved spectroscopy in time-dependent density functional theory: An exact condition, *Phys. Rev. Lett.* **114**, 183002 (2015).
- [60] K. Luo, J. I. Fuks, and N. T. Maitra, Studies of spuriously shifting resonances in time-dependent density functional theory, *The Journal of Chemical Physics* **145**, 044101 (2016), <http://dx.doi.org/10.1063/1.4955447>.
- [61] E. W. Draeger, X. Andrade, J. A. Gunnels, A. Bhatele, A. Schleife, and A. A. Correa, Massively parallel first-principles simulation of electron dynamics in materials, *J. Parallel Distrib. Comput.* **106**, 205 (2017).
- [62] I. Schelter and S. Kümmel, Accurate evaluation of real-time density functional theory providing access to challenging electron dynamics, *J. Chem. Theory Comput.* **14**, 1910 (2018), <https://doi.org/10.1021/acs.jctc.7b01013>.
- [63] H. O. Wijewardane and C. A. Ullrich, Real-time electron dynamics with exact-exchange time-dependent density-functional theory, *Phys. Rev. Lett.* **100**, 056404 (2008).
- [64] S. Raghunathan and M. Nest, Critical examination of explicitly time-dependent density functional theory for coherent control of dipole switching, *J. Chem. Theory and Comput.* **7**, 2492 (2011).
- [65] S. Raghunathan and M. Nest, The lack of resonance problem in coherent control with real-time time-dependent density functional theory, *J. Chem. Theory and Comput.* **8**, 806 (2012).
- [66] S. Raghunathan and M. Nest, Coherent control and time-dependent density functional theory: Towards creation of wave packets by ultrashort laser pulses, *J. Chem. Phys.* **136**, 064104 (2012).
- [67] B. F. Habenicht, N. P. Tani, M. R. Provorse, and C. M. Isborn, *J. Chem. Phys.* **141**, 184112 (2014).
- [68] E. E. Quashie, B. C. Saha, X. Andrade, and A. A. Correa, Self-interaction effects on charge-transfer collisions, *Physical Review A* **95**, 042517 (2017).
- [69] C.-Z. Gao, J. Wang, F. Wang, and F.-S. Zhang, Theoretical study on collision dynamics of $h^+ + \text{CH}_4$ at low energies, *The Journal of Chemical Physics* **140**, 054308 (2014).
- [70] C.-Z. Gao, P. M. Dinh, P.-G. Reinhard, and E. Suraud, Towards the analysis of attosecond dynamics in complex systems, *Phys. Chem. Chem. Phys.* **19**, 19784 (2017).
- [71] E. V. Boström, A. Mikkelsen, C. Verdozzi, E. Peretto, and G. Stefanucci, Charge separation in donor-c60 complexes with real-time green functions: The importance of nonlocal correlations, *Nano Lett.* **18**, 785 (2018), <https://doi.org/10.1021/acs.nanolett.7b03995>.
- [72] J. Krumland, A. M. Valencia, S. Pittalis, C. A. Rozzi, and C. Cocchi, Understanding real-time time-dependent density-functional theory simulations of ultrafast laser-induced dynamics in organic molecules, *J. Chem. Phys.* **153**, 054106 (2020).
- [73] C. M. Isborn and X. Li, Modeling the doubly excited state with time-dependent Hartree-Fock and density functional theories, *J. Chem. Phys.* **129**, 204107 (2008).
- [74] D. Dar, S. Roy, and N. T. Maitra, Curing the divergence in time-dependent density functional quadratic response theory, *The Journal of Physical Chemistry Letters* **14**, 3186 (2023).